Title
Operando STM study of the interaction of imidazolium-based ionic liquid with graphite

Authors
Wang, H
Wu, CH
Eren, B
et al.

Publication Date
2019-07-01

DOI
10.1016/j.ensm.2018.11.026

Peer reviewed

Operando STM Study of the Interaction of Imidazolium-based Ionic Liquid with Graphite

ABSTRACT

Understanding interactions at the interfaces of carbon with ionic liquids (ILs) is crucially beneficial for the diagnostics and performance improvement of electrochemical devices containing carbon as active materials or conductive additives in electrodes and ILs as solvents or additives in electrolytes. The interfacial interactions of three typical imidazolium-based ILs, 1-alkyl-3-methylimidazolium bis(trifluoromethanesulfonyl)imide (AMImTFSI) ILs having ethyl (C_2), butyl (C_4) and octyl (C_8) chains in their cations, with highly oriented pyrolytic graphite (HOPG) were studied *in-situ* by electrochemical scanning tunneling microscopy (EC-STM). The etching of HOPG surface and the exfoliation of graphite/graphene flakes as well as cation intercalation were observed at the HOPG/C_2MImTFSI interface. The etching also takes place in C_4MImTFSI at -1.5 V vs Pt but only at step edges with a much slower rate, whereas C_8MIm^+ cations adsorbs strongly on the HOPG surface under similar conditions with no observable etching or intercalation. The EC-STM observations can be explained by the increase in van der Waals interaction between the cations and the graphite surface with increasing length of alkyl chains.

Keywords: Electrochemical scanning tunneling microscope; ionic liquids; imidazolium; graphite

1. INTRODUCTION

Ionic liquids (ILs) are molten salts near room temperature composed of anions and cations sterically mismatched. In recent years, ILs have been used as electrolytes in energy storage devices such as batteries and supercapacitors,[1-3] thanks to their superior ionic conductivity, and good thermal and chemical stability. ILs are also introduced as additives in conventional carbonate-based electrolytes to improve the cycling stability and safety of rechargeable cells.[4-8] The most commonly used ILs in the electrochemical energy storage devices are those containing alkylammonium,[9-11] N-alkylpyrrolidinium,[4, 8] and N,N'-dialkylimidazolium[12-15] cations with alkyl chains of different length attached to the N atoms in the alkylammonium or aromatic rings.[16]

Carbon materials have been extensively used in electrochemical energy storage devices, primarily as electrode materials, for instance, graphite anode in lithium ion batteries (LIBs),[17] and porous carbon electrode in supercapacitors.[18, 19] The interaction between ILs and carbon materials including adsorption, etching, and intercalation may greatly influence the performance of relevant devices. The adsorption process of IL ions on carbon materials, for example, determines the capacitive behavior in electric double layer capacitors. The cation intercalation and cathodic etching at the graphite/IL interface can potentially interfere with the intercalation of lithium ions in LIBs. Understanding these interfacial processes is therefore crucially

beneficial for the diagnostics and performance improvement of relevant energy storage devices.

The structure of IL adsorption layer on graphite has been previously studied by both theory[1] and different experimental techniques such as scanning probe microscopy,[20] sum frequency generation,[21] high energy X-ray reflectivity.[22] It was found that the adsorption behavior of IL on graphite surface highly depends on the chemical structure of both cations and anions. X-ray diffraction (XRD) experiments confirmed the occurrence of intercalation of imidazolium or pyrrolidinium cations into graphite, where the N-containing rings of the cations align parallel to the graphene sheets and expand the graphite interlayer distance from 0.34 nm to 0.7 ~ 0.8 nm.[12, 14, 23, 24] Although the anodic etching of graphite by electrochemical oxidation has been well documented,[25-28] there are very few reports on the cathodic etching of graphite in ILs, among which is the STM study by Hu et al.[4], where cathodic etching of HOPG in N-methyl-N-propylpyrrolidinium bis(trifluoromethanesulfonyl)imide ($Py_{13}TFSI$) was observed and attributed to the decomposition of the $TFSI^-$ anions.

Electrochemical scanning tunneling microscopy (EC-STM) is a powerful *in-situ* technique for the characterization of solid/liquid interface under different potentials, including the interface between ILs and carbon materials such as highly oriented pyrolytic graphite (HOPG) or graphene.[4, 29] Herein, we report an EC-STM study on the adsorption, intercalation, and etching behavior of imidazolium-based ILs under open circuit potential (OCP) and cathodic

potentials at HOPG/IL interface and their dependence on the length of the alkyl chains in the aromatic cations.

2. EXPERIMENTAL

2.1. Materials

1-Ethyl-3-methylimidazolium bis(trifluoromethanesulfonyl)imide (C_2MImTFSI) and 1-Octyl-3-methylimidazolium bis(trifluoromethanesulfonyl)imide (C_8MImTFSI) both with 99.6% purity were purchased from Ionic Liquids Technologies (Io-Li-Tec, Germany). 1-Butyl-3-methylimidazolium bis(trifluoromethanesulfonyl)imide (C_4MImTFSI) with 98% purity was purchased from Sigma-Aldrich. The ILs used in this study all have the same anion and imidazolium cations, differing only in the alkyl chain length attached to the aromatic ring. Prior to electrochemical and STM experiments, the ILs were dried at 120 ^{o}C in a vacuum chamber to minimize the amount of water and oxygen contaminant in the IL. The HOPG (B-grade) sample obtained from the Institute of Metal Research, Chinese Academy of Sciences, was freshly cleaved for each set of electrochemical and STM experiments.

2.2. Electrochemical measurements

Cyclic voltammetry (CV) measurements were carried out inside an argon glove box using an Autolab PGSTAT 302N potentiostat with three-electrode control. The HOPG working electrode, with a diameter of 3 mm, was mounted

on a cylindrical hollow PEEK holder and sealed with a Viton ring. The counter and pseudo-reference electrodes were both made of Pt wires with diameters of 0.25 mm. All CV measurements started in the cathodic sweeping direction from OCP to -1.8 V vs Pt. Because all the STM experiments started on a freshly cleaved HOPG surface with no electrochemical pre-treatments, given the changes of HOPG surface observed in some STM measurements, only the first cycle of CV measurements was reported and discussed here.

2.3. EC-STM measurements

EC-STM measurements were performed using a Beetle-style scan-head and SPM100 controller from RHK Technology,[30] with the scanner mounted on top of a home-built electrochemical cell inside a sealed nitrogen chamber. Platinum wires were also used as both counter and pseudo-reference electrodes in STM experiments. A bipotentiostat (Pine Instrument Company, Model AFCBP1) was used to simultaneously control the sample potential and the bias voltage between sample and tip. Figure 1 shows a schematic diagram of the EC-STM setup. The imaging parameters: $V_t = V_{sample} - V_{tip}$, and I_t, are indicated in the figure captions. STM tips were prepared by electrochemically etching a Pt-Ir wire (0.25 mm in diameter), which was subsequently coated with Apiezon wax, except a few μm near the apex. Such coating step was necessary to minimize spurious currents from the solution background (compared to typically 10 pA tunneling current).

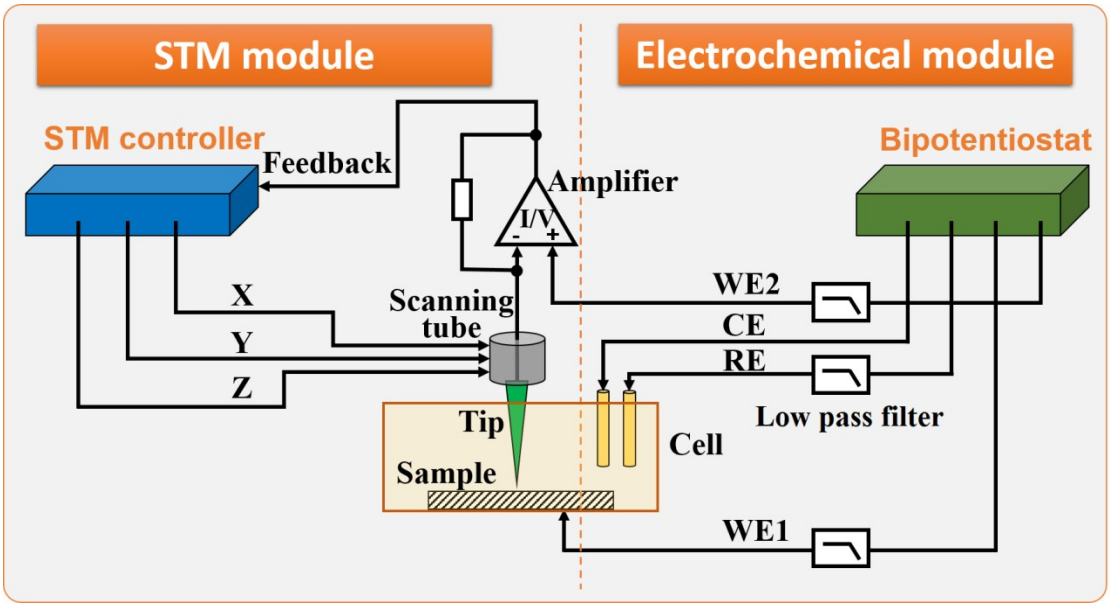

Figure 1. Schematic diagram of the EC-STM setup

3. RESULTS AND DICUSSION

3.1. Cyclic voltammetry

Figure 2 shows the first-cycle CV curves of HOPG electrode in all three ILs. The molecular structures of these ILs are illustrated in the insets. For C_2MImTFSI, a sharp increase in the cathodic current below -1.65 V vs Pt indicates the onset of massive cation decomposition and possibly simultaneous cation intercalation.[31] The cathodic peak at -0.9 V vs Pt, marked as C2a in Figure 2a, can be attributed to the reduction of water and oxygen residuals in the ILs, according to the electrochemical study by Randstrom et al.[31] The distinct feature seen at -1.78 V vs Pt in the anodic sweep, marked as A2, is possibly related to the de-intercalation of surviving cations.[4, 12] For C_4MImTFSI and C_8MImTFSI, similar impurity-related anodic peaks, marked as C4a and C8a respectively, can be seen between -0.9 and -

1.0 V vs Pt. In both cases however only mild increase in the cathodic current was observed beyond the C4a/C8a peaks and no anodic features related to the de-intercalation were present in the anodic sweep.

Another important observation is the color change in the C_2MImTFSI ILs, from initially colorless to brown when the potential was held at -2.0 V vs Pt. Such color change is due to the graphene sheets and/or graphite flakes detached from the HOPG surface and then dispersed in the bulk IL, as will be demonstrated later in the STM experiments. No such color change was observed in the C_4MImTFSI and C_8MImTFSI.

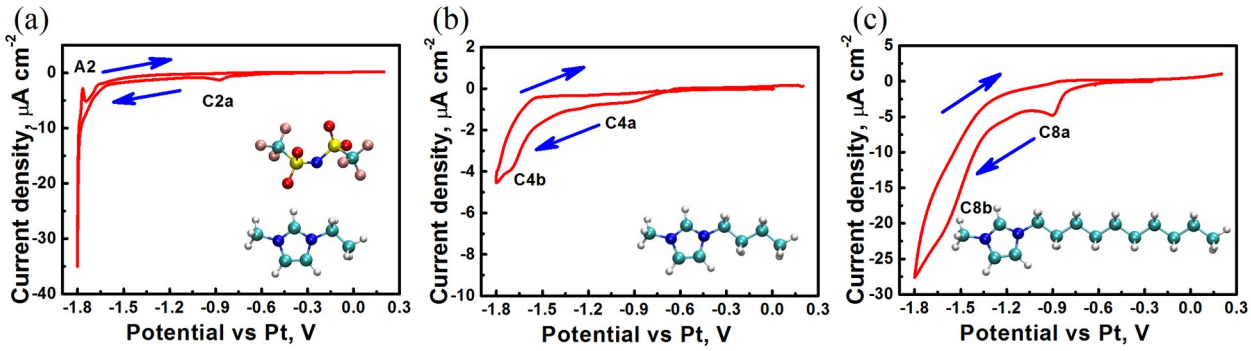

Figure 2. First-cycle CV curves of HOPG electrodes: (a) in C_2MImTFSI, (b) in C_4MImTFSI, and (c) in C_8MImTFSI, acquired with a scanning rate of 5 mV/s. The molecular structures of C_2MIm^+ and $TFSI^-$, C_4MIm^+, C_8MIm^+ are shown as insets, where H, C, N, O, F and S atoms are shown in gray, cyan, blue, red, ochre, and yellow, respectively.

3.2. Adsorption of $C_{2,4,8}$MImTFSI on HOPG

In C_2MImTFSI under OCP at low tunneling resistance (V_t = 50 mV, I_t = 50 pA), the STM image, shown in Figure 3a, reveals only the structure of clean graphite with no features related to the adsorption of either ion. This is in

contrast with intermittent-contact mode AFM results which suggest co-adsorption of cations and anions with well-defined structures on the HOPG surface.[32] The absence of IL-related features in our STM results is likely due to the weak adsorption of both ions at OCP and the close proximity of the tip to the surface that causes displacement of the molecular layer. In intermittent AFM contact mode, however, the dragging force to displace the molecules is much lower. After a factor 3 increase in tunneling resistance (V_t = 500 mV, I_t = 150 pA), which corresponds to an approximately 50 pm larger tip-surface separation, the adsorbed molecules could be sensed, evidenced by the presence of streaks in the image as shown in Figure 3b, resulting from the tip dragging the molecules. Operating at even bigger tip-sample distances was not possible owing to the tip instability at higher tip voltages. Increasing the electrostatic force between molecules and surface can potentially help to hold down the ions, but -1.5 V vs Pt, the lowest potential we tested here, is still not sufficient to immobilize the ions and no specific structure was observed, as shown in Figure 3c. Similar phenomena were observed at the HOPG/C_4MImTFSI interface.

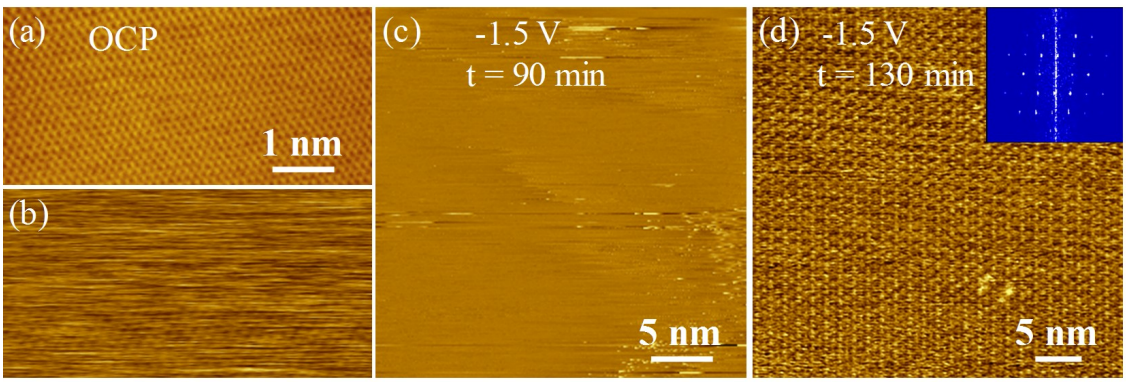

Figure 3. EC-STM images of the HOPG surface (a, b) in C_2MImTFSI under open cell potential, (c) in C_2MImTFSI under -1.5 V vs Pt, (d) in C_8MImTFSI under -1.5 V vs Pt. The insert in (d) is a corresponding Fast Fourier Transfer (FFT) image. Imaging parameters: (a) V_t = 50 mV, I_t = 50 pA; (b-d) V_t = 500 mV, I_t = 150 pA. Image sizes: (a, b) 6 × 3 nm^2; (c) 30 × 30 nm^2; (d) 40 × 40 nm^2.

In the case of C_8MImTFSI however, a periodic superstructure with 4-fold symmetry and 1.5 nm period was observed after 130 min scanning at -1.5 V vs Pt, as shown in Figure 3d. At such negative potentials, the first layer should be almost exclusively comprised of cations, as suggested by molecular dynamic simulations[33, 34] and AFM studies.[32, 35, 36] The observation of the undisturbed superstructure indicates the stronger interaction of C_8MIm^+ cations with HOPG substrate compared to C_2MIm^+ and C_4MIm^+, such that the adsorbed C_8MIm^+ cations now cannot be displaced by the STM tip. Given the structure difference in these three cations, we can attribute the increase in the adsorption strength to the stronger van der Waals (vdW) interaction of the cations with longer alkyl chains at the HOPG surface.[37, 38] The period of 1.5 nm is slightly smaller than the length of the C_8MIm^+ cation (~1.7 nm), suggesting that the alkyl chains of the cations lie almost parallel to the HOPG surface possibly with some overlap between neighboring alkyl chains.

It is worth pointing out that such self-assembly is actually a slow and dynamic process, possibly because of the high viscosity of ILs. As observed by Carstens et al.[29], the superstructure formed at HOPG/C_8MImTFSI interface keeps evolving in consecutive STM scans even when the potential was held

constant. This may explain why the superstructure we observed when holding the potential at -1.5 V for 130 min is different from the reported by Carstens et al.

3.3. Cathodic etching of the graphite surface in $C_{2,4,8}$MImTFSI

Because the ions are too mobile at HOPG/$C_{2,4}$MImTFSI interfaces and cannot be detected by STM, we examined in more detail the changes on the HOPG surface itself under different potentials. The STM images acquired in C_2MImTFSI (Figure 4) show rapid morphological change on the HOPG surface, already observable at potential as low as -0.5 V vs Pt. In the consecutive images acquired at -0.5 V vs Pt (Figure 4a-d), the formation of graphite flakes can be seen, typically starting at step edges (one example marked in white dashed line). These flakes are mobile and, together with the mobile ions, contribute to the streaks observed in the images.

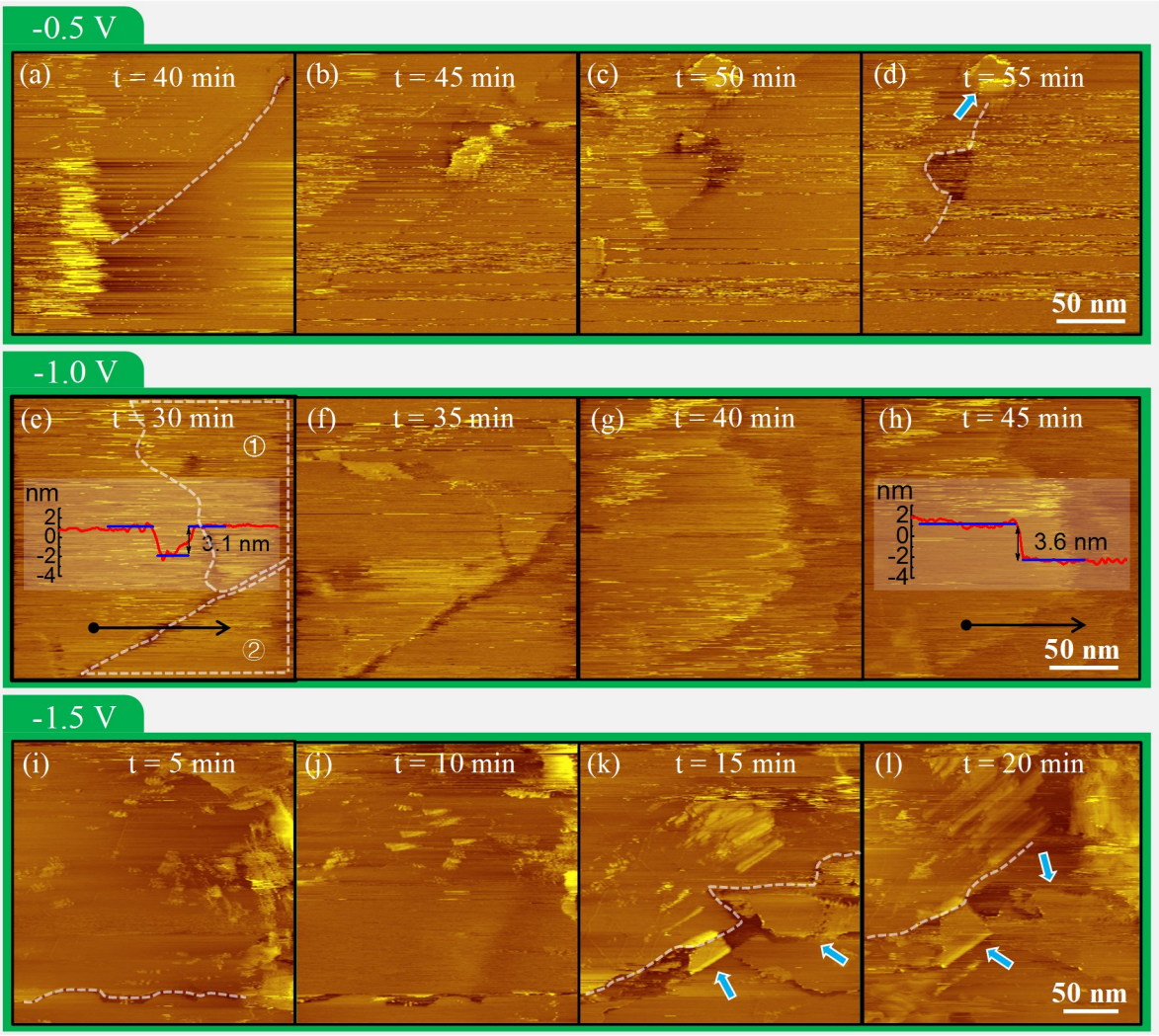

Figure 4. Time-lapse EC-STM images of the HOPG surface in C_2MImTFSI at (a-d) -0.5 V, (e-h) -1.0 V and (i-l) -1.5 V vs Pt. Imaging parameters: (a-h) V_t = 500 mV, I_t = 250 pA; (i-l) V_t = 500 mV, I_t = 200 pA. Image sizes: (a-h) 200 × 200 nm^2; (i-l) 250 × 250 nm^2. White dashed lines mark the graphite step edges where exfoliation and detachment of flakes were initiated. The blue arrows in (k) and (l) highlight some detached flakes. The insets in (e) and (h) show the height profiles along the black arrows in the corresponding images.

At -1.0 V vs Pt, cracking of HOPG surface and removal of two large flakes (marked 1 and 2 in Figure 4e) can be seen in consecutive images in Figure 4e-h. The initial trench in Figure 4e (at the center of the black arrow; 3.1 nm in depth) eventually evolved into a step edge of 3.6 nm in height after 15 min as shown in Figure 4h, while the graphite flake 2 on the right completely disappeared from the scan range. An even lower potential of -1.5V vs Pt leads to more severe surface cracking and exfoliation, producing more mobile graphite flakes, as can be seen in Figure 4i-k.

Similar STM experiments were performed in C_4MImTFSI and C_8MImTFSI. Unlike the case of C_2MImTFSI, neither severe cracking nor rapid exfoliation was observed in both ILs with longer alkyl chains. In C_4MImTFSI, instead we observed a very slow recession of external step edges (marked by white dashed line in Figure 5), at both -0.5 V (Figure 5a and b) and -1.5 V vs Pt (in a different area of the surface; Figure 5c and d). Some of the observed steps (marked in blue in Figure 5a and b) are internals steps (graphene flakes buried under the top layers)[39], which are not accessible from the solution and remained unchanged. The cross-edge profile along the arrow in Figure 5d, shows that the step height remains constant at 0.34 nm (the spacing between consecutive graphene layers), indicative of no intercalation of C_4MIm^+ cations between the graphene sheets.

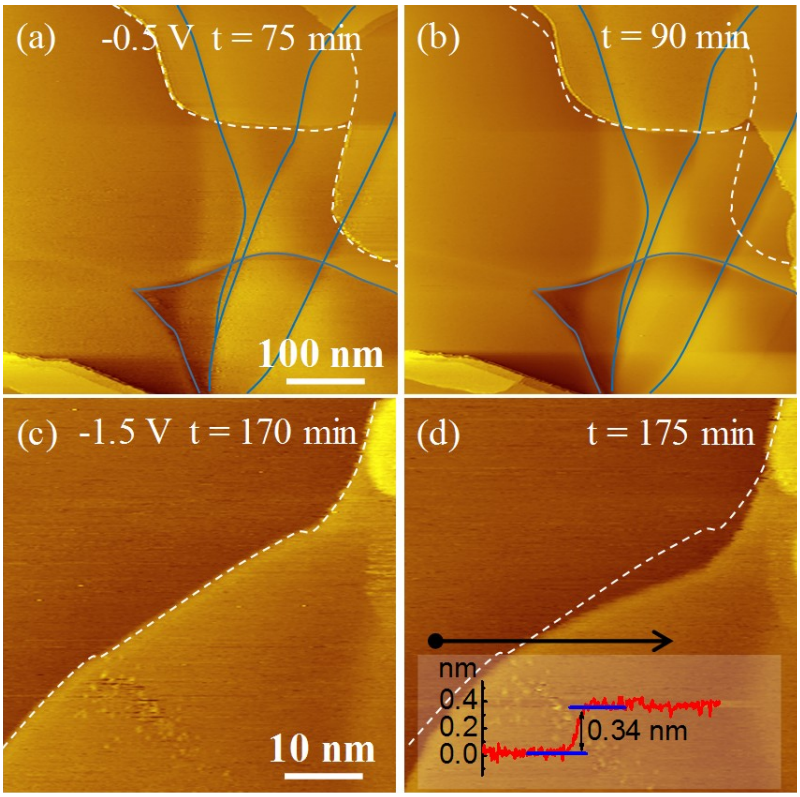

Figure 5. Time-lapse EC-STM images of the HOPG surface in C_4MImTFSI at (a, b) -0.5 V and (c, d) -1.5 V vs Pt. Imaging parameters: V_t = 50 mV, I_t = 100 pA. Image sizes: (a, b) 500 × 500 nm^2; (c, d) 50 × 50 nm^2. The initial positions of external step edges in (a) and (c) are marked with white dashed lines to help to visualize the changes with time. Internal step edges are marked in blue lines. The inset of (d) shows the height profile along the black arrow.

In C_8MImTFSI, we did not observe obvious step edge recession even at -1.5 V vs Pt, as shown in Figure 6. The height profile across the step edge marked by the black arrow remained unchanged after 15 min. The step height between the left and right flat areas is 0.47 nm, slightly larger than the distance between graphene sheets in HOPG (0.34 nm) but not enough to accommodate the C_8MIm^+ cations. The small jump in height (0.67 nm) right

at the edge can be caused by folded edge and/or by multiple images due to double-tip or even triple-tip asperities in this particular experiment.

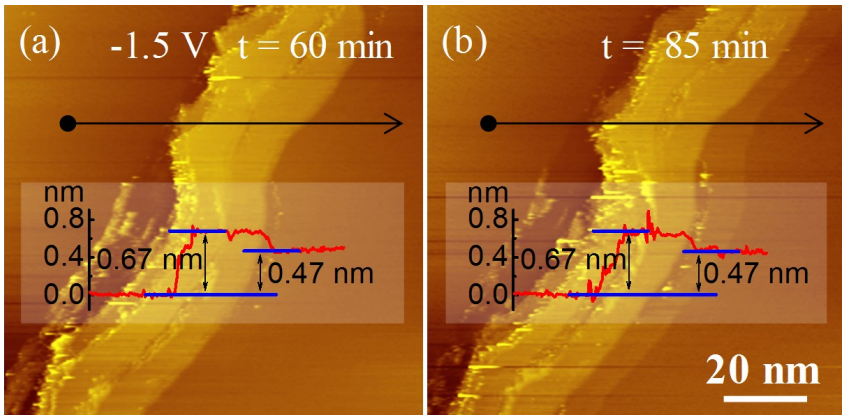

Figure 6. Time-lapse EC-STM images of the HOPG surface in C_8MImTFSI acquired at -1.5 V vs Pt. Imaging parameters: V_t = 500 mV, I_t = 50 pA. Image sizes are both 100 × 100 nm^2. A multiple tip effect is present in these images that produces 3 or more ghost images of the step edge. The insets in (a) and (b) show the height profiles along the black arrows in corresponding images.

3.4. Dependence of etching rate on the length of alkyl chains

Given the similarity in the molecular structure of these three ILs, it is reasonable to expect a similar chemical origin of any chemical attack of the graphite by the ILs. According to Hu et al.[4], such cathodic etching is induced by anion $TFSI^-$ decomposition, which can be further catalyzed by the reduction products of water/oxygen impurities.[31] However, our STM results show a clear dependence of the etching rate on the length of the alkyl chains. Based on the very different adsorption behavior observed in our STM

results, we can conclude that the adsorption strength of cations due to their different alkyl chains plays a crucial role in the etching process.

For the smallest cation C_2MIm^+, its adsorption on the graphite surface is the weakest among the three. As a result, the C_2MIm^+ cations are highly mobile, easily displaced by STM tips and thus cannot be detected by STM. Such high mobility of cations at the interface makes it easier for $TFSI^-$ anions or water/oxygen impurities to approach the graphite surface and decompose there, eventually causing the cathodic etching of graphite. The anodic de-intercalation peak (A2) observed in the CV curve points toward the occurrence of cation intercalation. Simultaneous etching and intercalation lead to rapid formation and detachment of graphite/graphene flakes from the HOPG surface in $C_2MImTFSI$ as we observed in the STM experiments, which also explains the color change of the $C_2MImTFSI$ IL when the potential was held at -2.0 V vs Pt.

Spontaneous cation intercalation and subsequent exfoliation at OCP has been observed by Atkins et al. in C_2MImAc and $C_2MImTFMS$,[40] while the spontaneous exfoliation was not observed in $C_2MImTFSI$ by these authors. The vdW interaction between graphene sheets can prevent them from sliding,[41] as well as exfoliating. But the electric field at sufficiently high negative potentials can drive the C_2MIm^+ cations in between graphite layers, especially through the etching cracks on the surface, then triggering the exfoliation.

For the cations with longer alkyl chains, C_4MIm^+ and C_8MIm^+, the stronger vdW interaction with the graphite surface makes them adsorb more strongly compared to C_2MIm^+, leading to the formation of the superstructure observed at C_8MImTFSI/HOPG interface. Stronger adsorption on the graphite surface will certainly reduce the mobility of the interfacial cations, impede the decomposition of $TFSI^-$ or impurities at the interface and consequently slow down the etching process. Indeed, instead of rapid exfoliation and intercalation, only slow recession of step edges was observed in C_4MImTFSI and no obvious change at HOPG/C_8MImTFSI interface. The stronger adsorption also seems to impact the intercalation behavior of the cations. The absence of anodic peaks in the CV curves of the two longer chain ILs, like the A2 peak in the CV curve of C_2MImTFSI, supports no or minimal intercalation at least down to -1.8V vs Pt, in line with the lack of any observed change in height with time in the STM images for C_4MImTFSI and C_8MImTFSI.

4. CONCLUSIONS

We studied the interaction of $C_{2,4,8}$MImTFSI with HOPG surface at OCP and cathodic conditions using EC-STM. It was found that the adsorption strength of the cations increases with the length of the alkyl chains because of increasing vdW interaction. The difference in adsorption strength has an important impact on the mobility of the cations at the HOPG/IL interfaces and consequently alters the rate of cathodic etching on graphite surface, leading to drastically different surface modifications in three ILs: etching and

exfoliation in C_2MImTFSI, slow step edge recession in C_4MImTFSI, and no observable change in C_8MImTFSI. Our results provide useful insights to help understand the mechanism of carbon/IL interfacial processes as well as diagnose the performance of electrochemical devices containing carbon as active materials or conductive additives in electrodes and ILs as solvents or additives in electrolytes.

ACKNOWLEDGEMENTS

This work was supported by the Office of Basic Energy Sciences (BES), Division of Materials Sciences and Engineering, of the U.S. Department of Energy (DOE) under Contract DE-AC02-05CH11231, through the Structure and Dynamics of Materials Interfaces program (FWP KC31SM). H.W., B.F. and H.-T. F. acknowledge the support from Harbin Institute of Technology through the Short-term Visiting Program and Natural Scientific Research Innovation Foundation (Grant no. 30620160007) and by the National Natural Science Foundation of China (Grant no. 51272051, 50872026). B.E. acknowledges financial support from the Swiss National Science Foundation (SNF) through Early Postdoctoral Mobility fellowship.

Data Availability

The raw data and processed data required to reproduce these findings are available to download from http://dx.doi.org/10.17632/brkjgjd234.1.

REFERENCES

1. M. V. Fedorov and A. A. Kornyshev, Ionic Liquids at Electrified Interfaces, *Chem. Rev.*, 2014, 114, 2978-3036.
2. M. Armand, F. Endres, D. R. MacFarlane, H. Ohno and B. Scrosati, Ionic-Liquid Materials for the Electrochemical Challenges of the Future, *Nat. Mater.*, 2009, 8, 621-629.
3. A. Lewandowski and A. Świderska-Mocek, Ionic Liquids as Electrolytes for Li-Ion Batteries - an Overview of Electrochemical Studies, *J. Power Sources*, 2009, 194, 601-609.
4. X. Hu, C. Chen, J. Yan and B. Mao, Electrochemical and in-Situ Scanning Tunneling Microscopy Studies of Bis(Fluorosulfonyl)Imide and Bis(Trifluoromethanesulfonyl)Imide Based Ionic Liquids on Graphite and Gold Electrodes and Lithium Salt Influence, *J. Power Sources*, 2015, 293, 187-195.
5. S. Rothermel, P. Meister, G. Schmuelling, O. Fromm, H. W. Meyer, S. Nowak, M. Winter and T. Placke, Dual-Graphite Cells Based on the Reversible Intercalation of Bis(Trifluoromethanesulfonyl)Imide Anions from an Ionic Liquid Electrolyte, *Energy Environ. Sci.*, 2014, 7, 3412-3423.
6. N. Wongittharom, C. H. Wang, Y. C. Wang, G. T. K. Fey, H. Y. Li, T. Y. Wu, T. C. Lee and J. K. Chang, Charge-Storage Performance of Li/$LiFePO_4$ Cells with Additive-Incorporated Ionic Liquid Electrolytes at Various Temperatures, *J. Power Sources*, 2014, 260, 268-275.
7. R. Lin, P.-L. Taberna, S. Fantini, V. Presser, C. R. Pérez, F. Malbosc, N. L. Rupesinghe, K. B. K. Teo, Y. Gogotsi and P. Simon, Capacitive Energy Storage from -50 to 100 °C Using an Ionic Liquid Electrolyte, *J. Phys. Chem. Lett.*, 2011, 2, 2396-2401.
8. A. Guerfi, S. Duchesne, Y. Kobayashi, A. Vijh and K. Zaghib, $LiFePo_4$ and

Graphite Electrodes with Ionic Liquids Based on Bis(Fluorosulfonyl)Imide $(FSI)^-$ for Li-Ion Batteries, *J. Power Sources*, 2008, 175, 866-873.

9. P. W. Ruch, M. Hahn, F. Rosciano, A. Holzapfel, H. Kaiser, W. Scheifele, B. Schmitt, P. Novak, R. Kotz and A. Wokaun, In Situ X-Ray Diffraction of the Intercalation of $(C_2H_5)_4N^+$ and BF_4^- into Graphite from Acetonitrile and Propylene Carbonate Based Supercapacitor Electrolytes, *Electrochim. Acta*, 2007, 53, 1074-1082.
10. X. Hao, P. Liu, Z. A. Zhang, Y. Q. Lai, X. Y. Wang, J. Li and Y. X. Liu, Tetraethylammonium Tetrafluoroborate as Additive to Improve the Performance of $LiFePO_4$/Artificial Graphite Cells, *Electrochem. Solid-State Lett.*, 2010, 13, A118-A120.
11. M. Galinski, A. Lewandowski and I. Stepniak, Ionic Liquids as Electrolytes, *Electrochim. Acta*, 2006, 51, 5567-5580.
12. M. Egashira, T. Tanaka, N. Yoshimoto and M. Morita, Electrode Reaction Concerning Imidazolium Cation and Graphite in Organic Solvent Electrolyte, *Solid State Ionics*, 2012, 219, 29-33.
13. M. M. Hantel, A. Płatek, T. Kaspar, R. Nesper, A. Wokaun and R. Kötz, Investigation of Diluted Ionic Liquid 1-Ethyl-3-Methyl-Imidazolium Tetrafluoroborate Electrolytes for Intercalation-Like Electrodes Used in Supercapacitors, *Electrochim. Acta*, 2013, 110, 234-239.
14. T. E. Sutto, T. T. Duncan and T. C. Wong, X-Ray Diffraction Studies of Electrochemical Graphite Intercalation Compounds of Ionic Liquids, *Electrochim. Acta*, 2009, 54, 5648-5655.
15. R. T. Carlin, H. C. Delong, J. Fuller and P. C. Trulove, Dual Intercalating Molten Electrolyte Batteries, *J. Electrochem. Soc.*, 1994, 141, L73-L76.
16. M. C. Buzzeo, R. G. Evans and R. G. Compton, Non-Haloaluminate Room-Temperature Ionic Liquids in Electrochemistry - a Review, *Chemphyschem*, 2004, 5, 1106-1120.
17. J. M. Tarascon and M. Armand, Issues and Challenges Facing Rechargeable Lithium Batteries, *Nature*, 2001, 414, 359-367.
18. P. Simon and Y. Gogotsi, Capacitive Energy Storage in Nanostructured

Carbon-Electrolyte Systems, *Acc. Chem. Res.*, 2013, 46, 1094-1103.

19. Y. W. Zhu, S. Murali, M. D. Stoller, K. J. Ganesh, W. W. Cai, P. J. Ferreira, A. Pirkle, R. M. Wallace, K. A. Cychosz, M. Thommes, D. Su, E. A. Stach and R. S. Ruoff, Carbon-Based Supercapacitors Produced by Activation of Graphene, *Science*, 2011, 332, 1537-1541.
20. R. Atkin and G. G. Warr, Structure in Confined Room-Temperature Ionic Liquids, *J. Phys. Chem. C*, 2007, 111, 5162-5168.
21. S. Baldelli, Interfacial Structure of Room-Temperature Ionic Liquids at the Solid–Liquid Interface as Probed by Sum Frequency Generation Spectroscopy, *J. Phys. Chem. Lett.*, 2012, 4, 244-252.
22. M. Mezger, H. Schroder, H. Reichert, S. Schramm, J. S. Okasinski, S. Schoder, V. Honkimaki, M. Deutsch, B. M. Ocko, J. Ralston, M. Rohwerder, M. Stratmann and H. Dosch, Molecular Layering of Fluorinated Ionic Liquids at a Charged Sapphire (0001) Surface, *Science*, 2008, 322, 424-428.
23. H. Y. Zhang, Y. Y. Wu, W. Sirisaksoontorn, V. T. Remcho and M. M. Lerner, Preparation, Characterization, and Structure Trends for Graphite Intercalation Compounds Containing Pyrrolidinium Cations, *Chem. Mater.*, 2016, 28, 969-974.
24. T. E. Sutto, P. C. Trulove and H. C. De Long, Direct X-Ray Diffraction Evidence for Imidazolium Intercalation into Graphite from an Ionic Liquid, *Electrochem. Solid-State Lett.*, 2003, 6, A50-A52.
25. L. Cui, Y. Xu, B. Liu, W. Yang, Z. Song and J. Liu, Well-controlled preparation of evenly distributed nanoporous HOPG surface via diazonium salt assisted electrochemical etching process, *Carbon*, 2016, 102, 419-425.
26. K. J. Aoki, H. Wang, J. Chen and T. Nishiumi, Formation of graphite oxide nano-disks by electrochemical oxidation of HOPG, *Electrochim. Acta*, 2014, 130, 381-386.
27. Y.-R. Shin, S.-M. Jung, I.-Y. Jeon and J.-B. Baek, The oxidation mechanism of highly ordered pyrolytic graphite in a nitric acid/sulfuric acid mixture,

Carbon, 2013, 52, 493-498.

28. P. R. Singh and X. Zeng, Size-Dependent Intercalation of Ions into Highly Oriented Pyrolytic Graphite in Ionic Liquids: An Electrochemical Atomic Force Microscopy Study, *J. Phys. Chem. C*, 2011, 115, 17429-17439.
29. T. Carstens, R. Gustus, O. Höfft, N. Borisenko, F. Endres, H. Li, R. J. Wood, A. J. Page and R. Atkin, Combined STM, AFM, and DFT Study of the Highly Ordered Pyrolytic Graphite/1-Octyl-3-Methyl-Imidazolium Bis(Trifluoromethylsulfonyl)Imide Interface, *J. Phys. Chem. C*, 2014, 118, 10833-10843.
30. RHK Technology, www.rhk-tech.com. 1050 E. Maple Road, Troy, MI 48083, USA.
31. S. Randstrom, M. Montanino, G. B. Appetecchi, C. Lagergren, A. Moreno and S. Passerini, Effect of Water and Oxygen Traces on the Cathodic Stability of N-Alkyl-N-Methylpyrrolidinium Bis(Trifluoromethanesulfonyl)Imide, *Electrochim. Acta*, 2008, 53, 6397-6401.
32. A. Elbourne, S. McDonald, K. Voichovsky, F. Endres, G. G. Warr and R. Atkin, Nanostructure of the Ionic Liquid-Graphite Stern Layer, *ACS Nano*, 2015, 9, 7608-7620.
33. J. M. Black, D. Walters, A. Labuda, G. Feng, P. C. Hillesheim, S. Dai, P. T. Cummings, S. V. Kalinin, R. Proksch and N. Balke, Bias-Dependent Molecular-Level Structure of Electrical Double Layer in Ionic Liquid on Graphite, *Nano Lett.*, 2013, 13, 5954-5960.
34. K. Kirchner, T. Kirchner, V. Ivanistsev and M. V. Fedorov, Electrical Double Layer in Ionic Liquids: Structural Transitions from Multilayer to Monolayer Structure at the Interface, *Electrochim. Acta*, 2013, 110, 762-771.
35. B. McLean, H. Li, R. Stefanovic, R. J. Wood, G. B. Webber, K. Ueno, M. Watanabe, G. G. Warr, A. Page and R. Atkin, Nanostructure of [Li(G4)] TFSI and [Li(G4)] NO_3 Solvate Ionic Liquids at HOPT and Au(111) Electrode Interfaces as a Function of Potential, *Phys. Chem. Chem. Phys.*, 2015, 17, 325-333.

36. H. Li, R. J. Wood, F. Endres and R. Atkin, Influence of Alkyl Chain Length and Anion Species on Ionic Liquid Structure at the Graphite Interface as a Function of Applied Potential, *J. Phys.: Condens. Matter*, 2014, 26, 284115.
37. Q. Chen, H.-J. Yan, C.-J. Yan, G.-B. Pan, L.-J. Wan, G.-Y. Wen and D.-Q. Zhang, STM Investigation of the Dependence of Alkane and Alkane ($C_{18}H_{38}$, $C_{19}H_{40}$) Derivatives Self-Assembly on Molecular Chemical Structure on HOPG Surface, *Surf. Sci.*, 2008, 602, 1256-1266.
38. S. X. Yin, C. Wang, Q. M. Xu, S. B. Lei, L. J. Wan and C. L. Bai, Studies of the Effects of Hydrogen Bonding on Monolayer Structures of $C_{18}H_{37}X$ (X = OH, SH) on HOPG, *Chem. Phys. Lett.*, 2001, 348, 321-328.
39. H. Lee, H. B. R. Lee, S. Kwon, M. Salmeron and J. Y. Park, Internal and External Atomic Steps in Graphite Exhibit Dramatically Different Physical and Chemical Properties, *ACS Nano*, 2015, 9, 3814-3819.
40. A. Elbourne, B. McLean, K. Voitchovsky, G. G. Warr and R. Atkin, Molecular Resolution in Situ Imaging of Spontaneous Graphene Exfoliation, *J. Phys. Chem. Lett.*, 2016, 7, 3118-3122.
41. X. Feng, S. Maier and M. Salmeron, Water Splits Epitaxial Graphene and Intercalates, *J. Am. Chem. Soc.*, 2012 134 5662-5668.